Supporting Online Material for

A Manganese Hydride Molecular Sieve for Practical Hydrogen Storage Under Ambient Conditions

Leah Morris, James J. Hales, Michel L. Trudeau, Peter Georgiev, Jan Peter Embs, Juergen Eckert, Nikolas Kaltsoyannis, David M. Antonelli*

*To whom correspondence should be addressed: d.antonelli@lancaster.ac.uk

Supporting Materials:

Materials and Methods

Figures S1-S30

Tables S1-S11

Characterization

Infrared Spectroscopy:

Infrared spectroscopy was conducted on a Perkin Elmer Spectrum RX1 using KBr. Prior to analysis, the IR grade KBr was oven dried overnight at 393 K to remove any residual water. A blank sample of KBr was ground in an oven-dried pestle and mortar in the glovebox and then compressed to form a disc. A background was taken of the blank KBr disc. Approximately 5 mg of sample was ground with 200 mg KBr in the

glovebox and then compressed to form a disc. The spectrum of KBr was then subtracted from that of the sample.

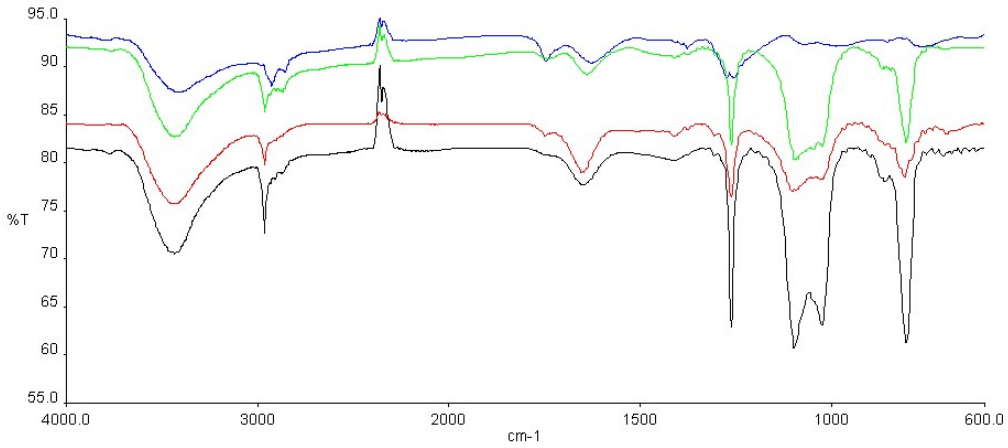

Fig S1. Infrared spectrum of KMH-1 as synthesized (black), KMH-1 after 1st hydrogenation (red), after 2nd hydrogenation (green), KMH-1 after cycling (blue).

Thermogravimetric Analysis (TGA):

The thermogravimetric analysis (TGA) and differential thermal analysis (DTA) was performed in a STA 449C analyzer from Netzsch under a flow of dried air at 10 K min^{-1} up to 973 K. Argon was also used to protect the balance section. The powder was partially sealed in a Cu pan inside an Ar glove box at 0.3 ppm of O_2 to minimize material reaction prior to reaction inside the thermal analyzer. A correction was performed to subtract the air reaction of the Cu pan itself. TGA and DTA plots are shown in Figures S2, S3 and S4. The TGA of **KMH-1 as synthesized** shows a steady decrease in mass between 25 and 250 °C. There are two exotherms in the DTA curve at about 212 and 270 °C. At 400 °C the mass loss was 50 %. Above 400 °C the mass starts increasing again as the material starts to oxidize. For **KMH-1 after 2nd**

hydrogenation, the mass of the material decreases steadily between 25 and 215 °C where it starts to plateau until the material retains 73.5% of its original weight. This decrease of 26.5% mass is attributed to loss of the remaining hydrocarbon from the material. The DTA curve shows three major exotherms at 238, 460, and 591 °C that could be due in part to the formation of Mn oxidation products as we also observe an increase in mass above 310 °C. Finally, the TGA for **KMH-1 after cycling** shows no mass loss but rather an increase of about 20 % from RT to 700 °C due to oxidation, consistent with very little hydrocarbon left in this sample. The DTA curve shows four major exotherms at 300, 360, 547 and 600 °C that could be due to the formation of Mn oxidation products. This data provides evidence of sequential mass loss from the hydrogenation steps originating from step-wise removal of the hydrocarbon ligands by hydrogenolysis.

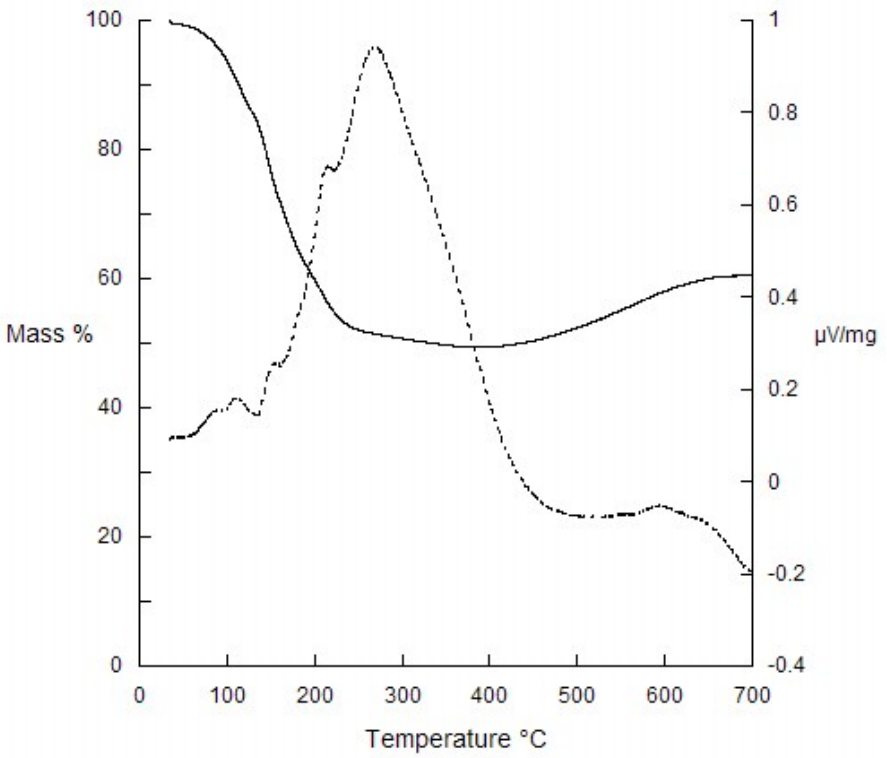

Fig S2. TGA (solid line) and DTA (dashed line) curves of KMH-1 as synthesized.

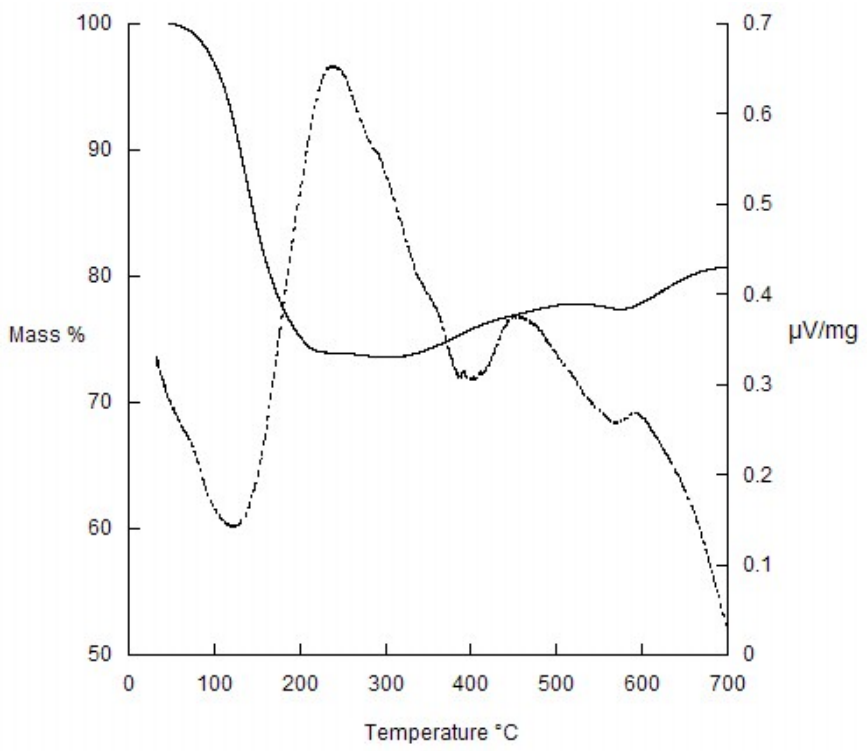

Fig S3. TGA (solid line) and DTA (dashed line) curves of KMH-1 after 2nd hydrogenation.

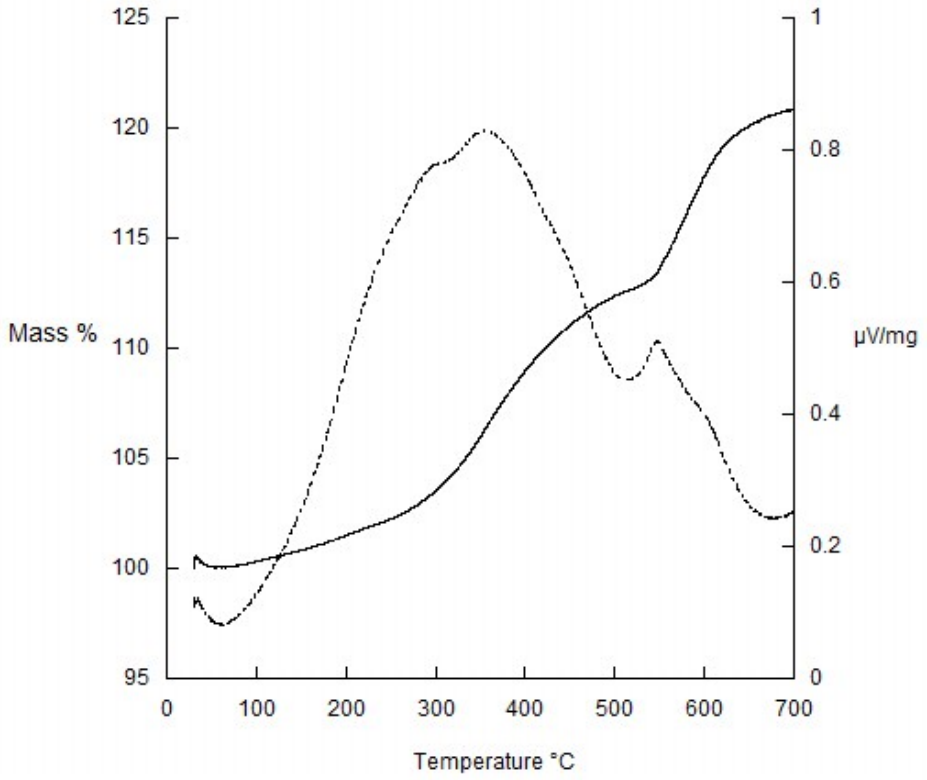

Fig S4. TGA (solid line) and DTA (dashed line) curves of KMH-1 after cycling

Nitrogen Adsorption:

Nitrogen adsorption and desorption data were collected at 77 K on a Micromeritics ASAP 2020. The BET surface area was calculated from points in the 0.1–0.3 P/P_0 range. The data is shown below in Figures S5-S8 and Table S1. For **KMH-1 as synthesized** the Branauer-Emmet-Teller (BET) surface area was 1.2 m^2/g. For **KMH-1 after 1st hydrogenation** and **KMH-1 after 2nd hydrogenation** the surface area increased to 6 and 66 m^2/g, respectively, with an increase in both meso- and micropore volume in **KMH-1 after 2nd hydrogenation**. The increase in surface area and porosity after each hydrogenation is due to removal of residual hydrocarbon template from the material as supported by the IR and formation of a porous manganese hydride structure. The formation of a templated incipient pore structure in the as-synthesized KMH-1 likely occurs during precipitation from the non-polar alkane solvent via an inverse micelle mechanism (*19*) (Fig. 1B). After 54 hydrogenation cycles, accompanied by an increase of the M-H stretch intensity in the IR and decrease in intensity of the C-H stretch, the BET surface area of **KMH-1 after cycling** was 257 m^2/g with the shape of the isotherm consistent with a mixture of micropores and mesopores with a broad pore size distribution.

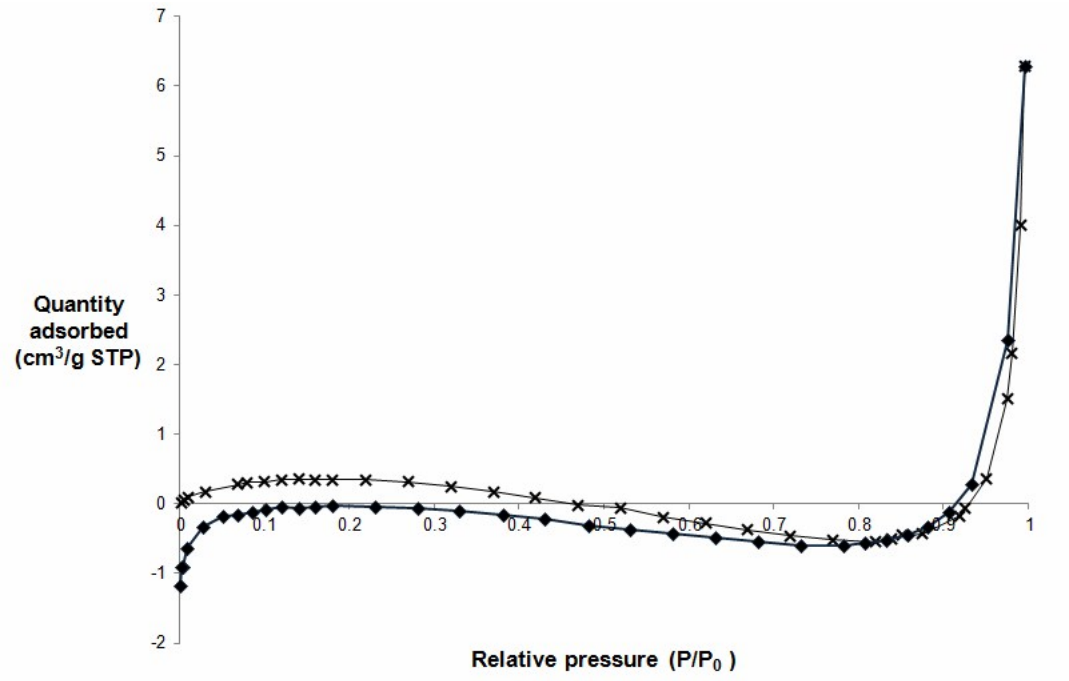

Fig S5. Nitrogen adsorption (crosses)-desorption (diamonds) isotherms of KMH-1 as synthesized recorded at 77 K.

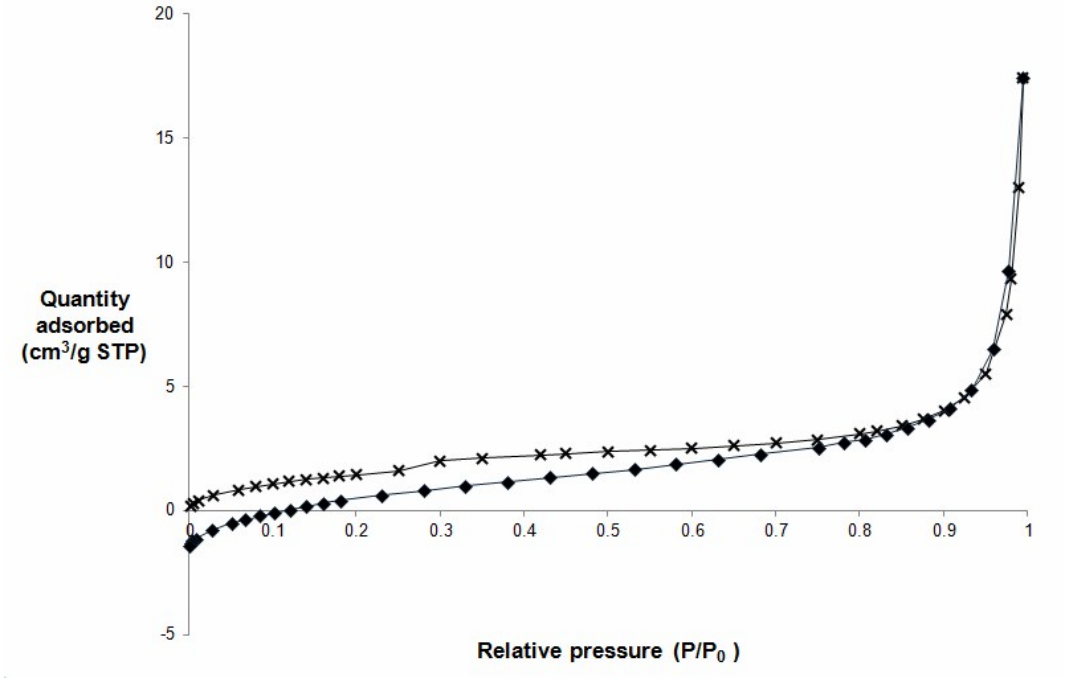

Fig S6. Nitrogen adsorption (crosses)-desorption (diamonds) isotherms of KMH-1 after 1st hydrogenation recorded at 77 K.

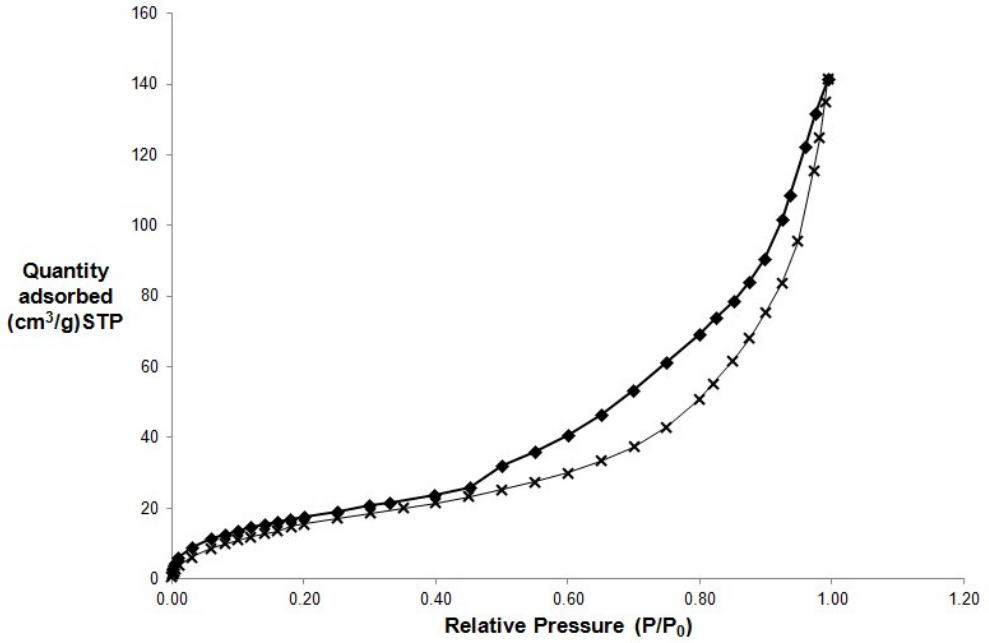

Fig S7. Nitrogen adsorption (crosses)-desorption (diamonds) isotherms of KMH-1 after 2nd hydrogenation recorded at 77 K

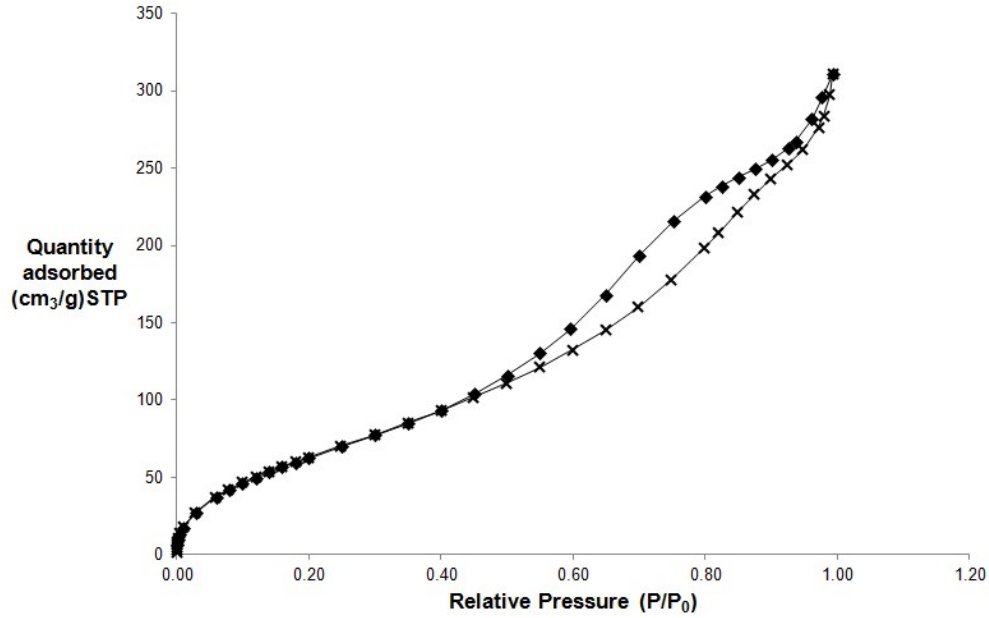

Fig S8. Nitrogen adsorption (crosses)-desorption (diamonds) isotherms of KMH-1 after cycling.

Sample	BET surface area (m^3/g)	Pore volume (cm^3/g)	Average BJH desorption pore size (Å)
KMH-1 as synthesised	1.2	0.003	n/a
KMH-1 after 1st hydrogenation	6	0.009	23.8
KMH-1 after 2nd hydrogenation	66	0.09	35.3
KMH-1 after cycling	257	0.3	49.3

Table S1. Porosity data for KMH-1 materials

Electron Microscopy (STEM): High resolution Electron Microscopy was performed at 200 kV on an HD-2700 dedicated Scanning Transmission Electron Microscope (STEM) from Hitachi, equipped with a cold field emitter equipped and a CEOS Cs corrector. A small amount of powder was placed onto a copper grid covered with a carbon layer having regular hole with a diameter of 1.2 μm. The powder was deposited on the grid inside an Ar glove box at 0.3 ppm of O_2. After that, the grid was mounted on a TEM holder having a special cover that isolates the sample from the air. The holder was then placed in the STEM goniometer and the sample region was evacuated three times before retracting the cover and inserting the sample inside the STEM. Observation was made in Secondary Electron mode (SE).

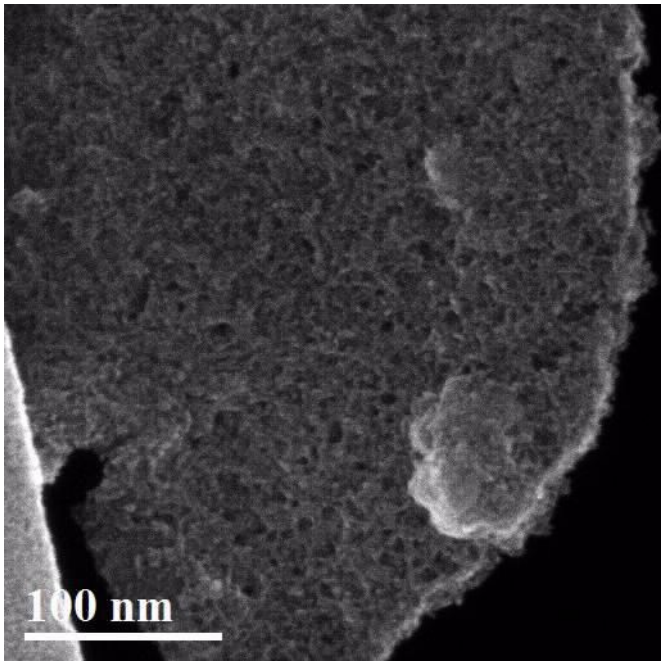

Fig S9. STEM-SE image of **KMH-1 after 2nd hydrogenation** at a scale of 100 nm (magnification 350 kX)

Powder XRD:

The Powder X-Ray Diffraction (PXRD) analysis was performed by placing a small amount of powder on a thin glass substrate cover with two-sided tape inside a glovebox. The powder-glass sample was then mounted inside an airtight specimen holder from Bruker. The XRD spectrum was recorded using a Bruker DaVinci diffractometer equipped with a Vantec-1 Position sensitive detector using Cu Kα radiation. The three large reflections at 9,69°, 11,26° and 19,98° are due to the dome itself.

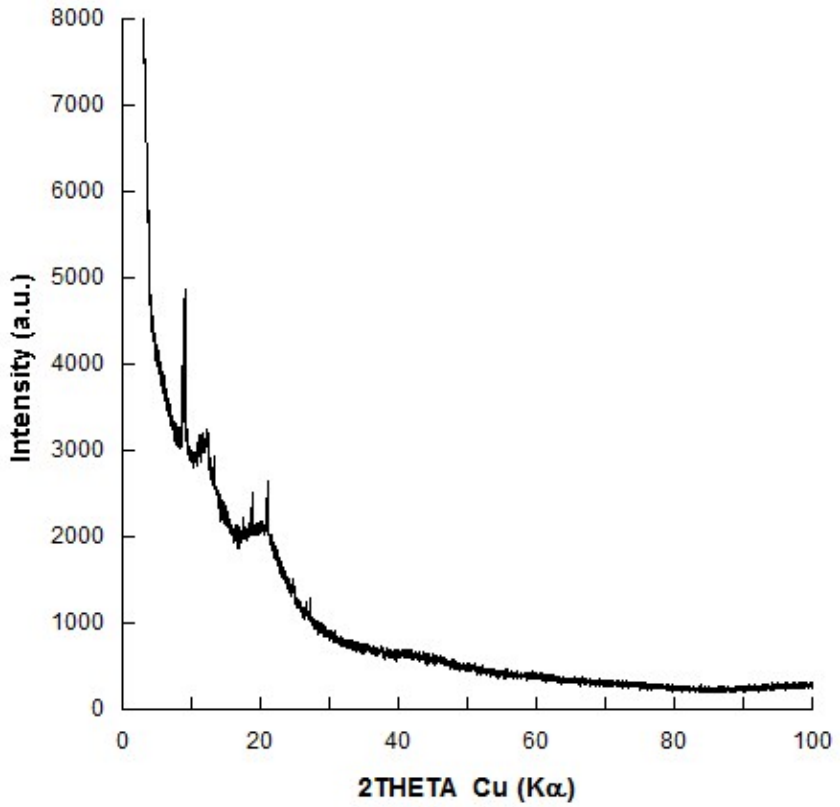

Fig S10. PXRD of KMH-1 as synthesized.

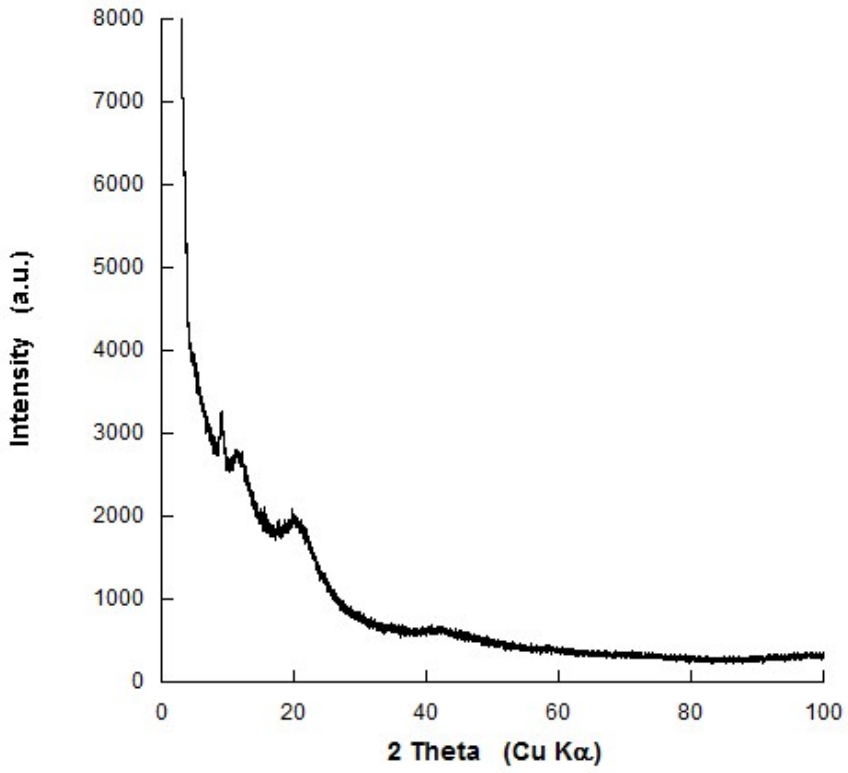

Fig S11. PXRD of KMH-1 after 2nd hydrogenation.

Energy Dispersive X-ray Spectroscopy (EDX): STEM EDS analysis was performed using a 60 mm^2 silicon drift detector from Bruker. Only Mn, Mg, Cl and S were used for obtaining semi-quantitative values of the concentration. Cu, Si, Al, Zr and Fe are artefacts from the sample holder, grid and pole piece.

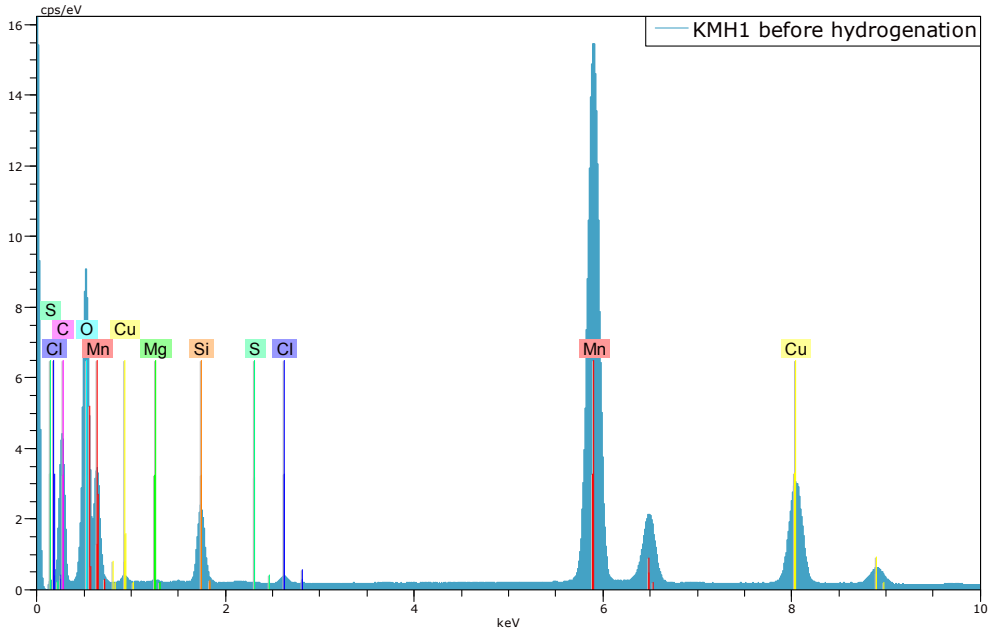

Fig S12. EDS plot of KMH-1 as synthesized

El	AN	Series	Net unn. C [wt.%]	norm. C [wt.%]	Atom. C [at.%]	Error (1 Sigma) [wt.%]
Mn	25	K-series	1454208	99,00	99,00	98,35	3,00

Cl	17	K-series	13907	0,77	0,77	1,18
0,05						
Mg	12	K-series	2339	0,13	0,13	0,29
0,03						
S	16	K-series	2019	0,11	0,11	0,18
0,03						
C	6	K-series	147763	0,00	0,00	0,00
0,00						
Cu	29	K-series	318882	0,00	0,00	0,00
0,00						
Si	14	K-series	118736	0,00	0,00	0,00
0,00						
Zr	40	L-series	3213	0,00	0,00	0,00
0,00						
Fe	26	K-series	9464	0,00	0,00	0,00
0,00						
O	8	K-series	324076	0,00	0,00	0,00
0,00						
Al	13	K-series	1937	0,00	0,00	0,00
0,00						
Total:				100,00	100,00	100,00

Table S2. EDS data for KMH-1 as synthesized

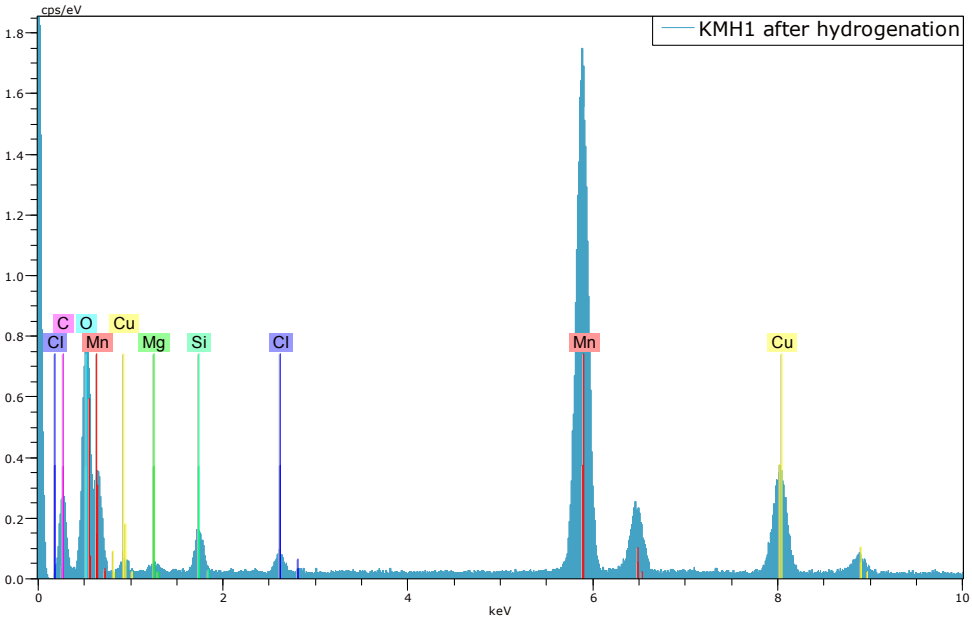

Fig S13. EDS plot of KMH-1 after 2nd hydrogenation.

El	AN	Series	Net unn. C [wt.%]	norm. C [wt.%]	Atom. C [at.%]	Error (1 Sigma) [wt.%]
Mn	25	K-series	45824	97,32	97,32	95,56	2,98
Cl	17	K-series	1241	2,14	2,14	3,25	0,12
Mg	12	K-series	317	0,54	0,54	1,19	0,06
C	6	K-series	3333	0,00	0,00	0,00	0,00
Cu	29	K-series	10404	0,00	0,00	0,00	0,00
Si	14	K-series	2574	0,00	0,00	0,00	0,00

Zr	40	L-series	0	0,00	0,00	0,00
0,00						
Fe	26	K-series	632	0,00	0,00	0,00
0,00						
O	8	K-series	10301	0,00	0,00	0,00
0,00						
Al	13	K-series	144	0,00	0,00	0,00
0,00						
S	16	K-series	0	0,00	0,00	0,00
0,00						
Total:				100,00	100,00	100,00

Table S3. EDS data for KMH-1 after 2nd hydrogenation.

X-ray Photoelectron Spectroscopy (XPS):

The XPS analysis was performed using a PHI-5500 spectrometer using monochromated Al Kα radiation. The positions of the peaks were referenced to surface C–C or C–H bound at 284.8 eV. The powder was placed on the XPS holder inside an Ar glove box and transferred under Ar to the XPS intro chamber without any exposure to air. For insulating materials, an electron-flooding gun was used to compensate the surface charges. The different chemical contributions for each spectrum were obtained using CasaXPS. **KMH-1 after 2nd hydrogenation** shows a broad emission in the Mn 2p3/2 region centered at 641 eV, which can be simulated by multiple species spanning from 640-643 eV, in addition to an emission at 643.9 eV (Fig. 2B). The major emissions centered around 641 eV can be attributed to an Mn(II) species by comparison to the emission for $MnCl_2$ at 641.9 eV (*20*) as well as substantial emissions from 640-641 eV due to Mn (I) species (*20*). The broad

distribution of sites is expected from the amorphous nature of the material and suggests a non-stoichiometric Mn(II)-Mn(I) formulation. The low intensity shoulder at 643.89 eV can be assigned to a Mn(IV) species produced by trace oxidation by comparison to the emission observed for MnO_2 at 643.4 eV (*21*). A similar distribution of oxidation states is observed in the XPS of **KMH-1 as synthesized** (S14) confirming that hydrogenation has little effect on the distribution of oxidation states of the Mn center.

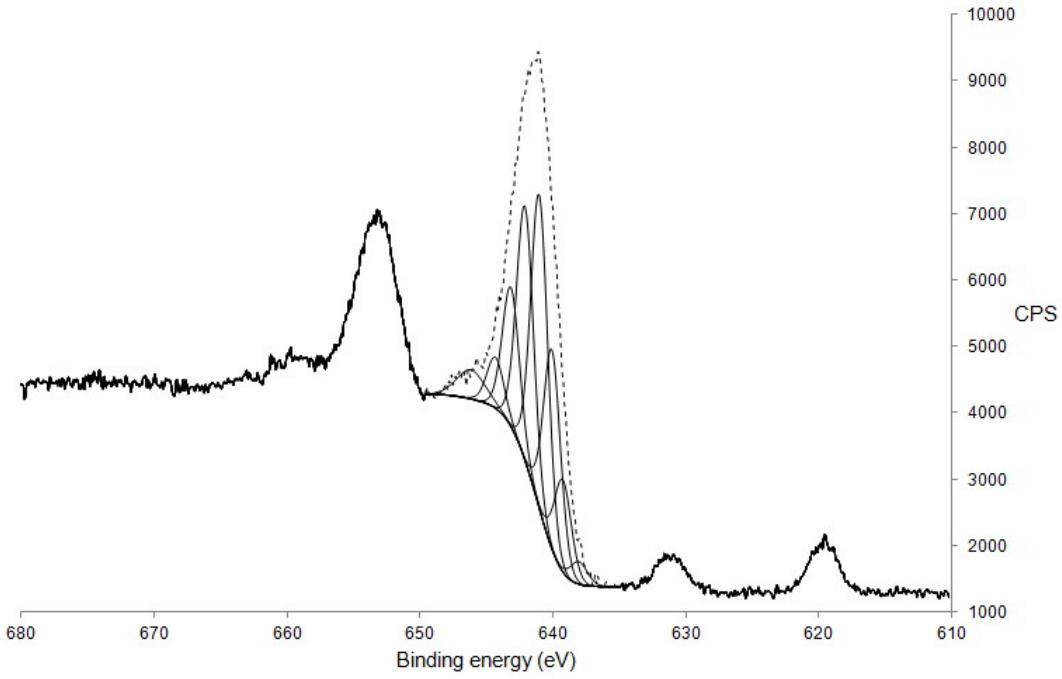

Fig S14. Peak fitting of manganese 2p1/2 and 2p3/2 region of XPS of **KMH-1 as synthesized**.

Hydrogen adsorption measurements:

Excess hydrogen adsorption isotherms were obtained by using a computer controlled gas sorption Sieverts apparatus manufactured by Setaram (PCT-Pro). High purity

hydrogen (Grade 6, 99.9999% purity) purchased from Air Liquide was used. Stainless steel spacers were added to the sample holder along with the material to reduce excess void space. The void space of the sample was calculated by performing a helium volume calibration at 298 K using 5 each adsorption and desorption points (total of 10), with outlying values discarded and rerun. An excess hydrogen adsorption measurement, which is the difference in the amount of fluid in the system and the amount that would be present at the same temperature and pressure in the absence of adsorption (*44*), on a 200 mg standard AX-21 sample (0.65 wt% at 70 bar and 298 K) was performed to ensure correct functioning of the instrument (Fig. S15). This measurement is necessary to ensure the accuracy of the isotherms and eliminate the possibility of systematic volume calibration errors. By comparison, the reported gravimetric excess hydrogen adsorption capacity of carbon AX-21 is 0.3 wt% at 35 bar (*25*). This corresponds to 0.6 wt% at 70 bar which extrapolates to an error of ±0.07 wt% ((0.65 - 0.6)*100/70) at 100 bar H_2 with a 200 mg sample size. A 200 mg sample size of carbon AX-21 gives ca. 2 mmol of excess adsorption at 120 bar, so we can be confident that 2 mmol uptake at this pressure by any sample regardless of the mass is a sufficient total hydrogen uptake to eliminate any virtual adsorption artifacts due to systematic volume calibration errors. All materials were thus tested at this same level of total adsorption (2–3 mmol at 120 bar) for consistency and to ensure accuracy of isotherms obtained, and the system rigorously leak-tested before every measurement. A cycle of ten isotherms of titanocene (100 mg), which turns from green to orange on exposure to oxygen, was also taken to rule out any oxidation of the sample during the measurement process. To ensure repeatability of the synthesis process and further validate the excess adsorption measurements, a sample of **KMH-1 after 1st hydrogenation** was generated on-site at Hydro Quebec and tested on a

second Setaram PCT Pro under identical conditions. The PCT cycle life measurement was conducted at room temperature (Fig. S16). This consisted of 54 repeated cycles of adsorption from 0–120 bar and desorption starting at 120 back down to 0 bar. In between each adsorption–desorption cycle the sample was evacuated for 5 minutes at room temperature. For the cycle life measurement a shorter equilibration time (1 minute compared to 5 minutes) and higher ΔP (30 compared to 5-10) were used to speed up the measurement in order to obtain a high number of cycles in a reasonable time frame. The total measurement time for 54 cycles was 12 days. After the cycling measurement was complete the material was removed from the PCT-Pro and the final weight of the sample was recorded (22 mg) and a new isotherm was taken with 10 new volume calibrations.

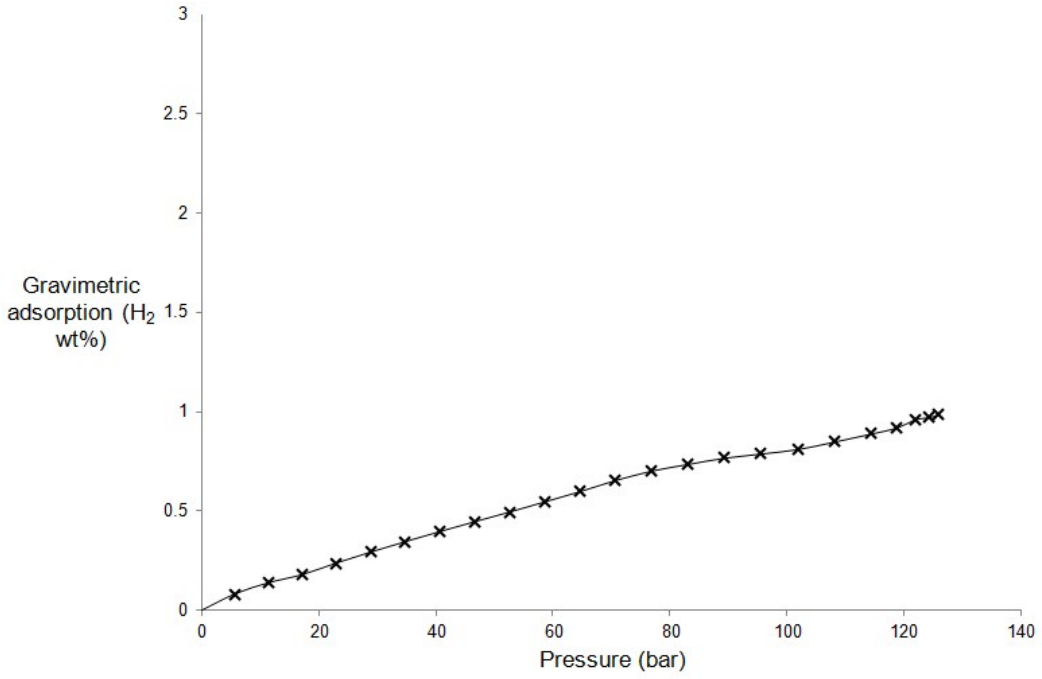

Fig S15a. Excess hydrogen adsorption isotherm for carbon AX-21 (200 mg) recorded at 298K. Total excess adsorption at 120 bar = 2 mmol

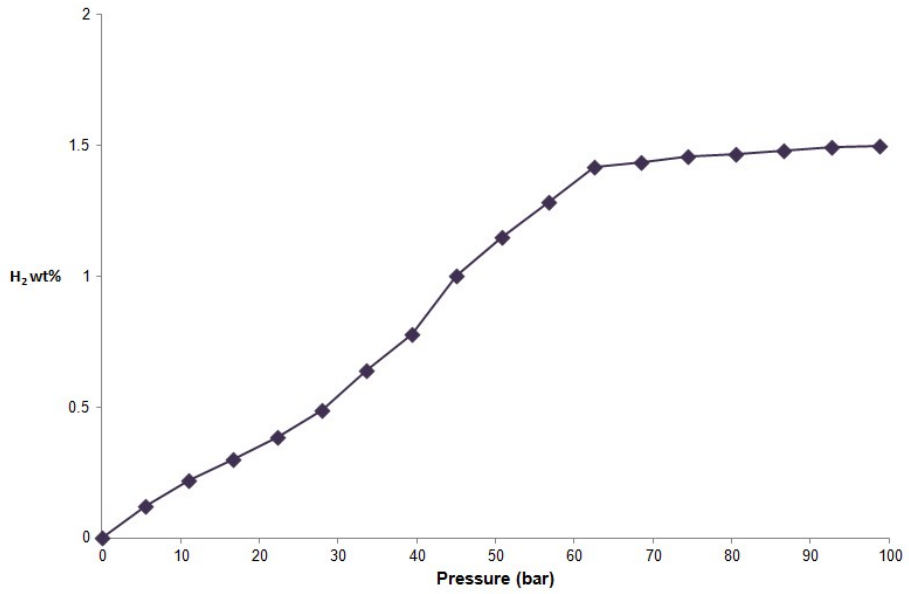

Fig S15b. Excess hydrogen adsorption isotherm recorded at 298 K for 40 mg sample of "fouled" **KMH-1 after 2nd hydrogenation** synthesized using oxidized "green" (bis)neopentyl manganese solution. Total excess adsorption at 100 bar = 0.6 mmol

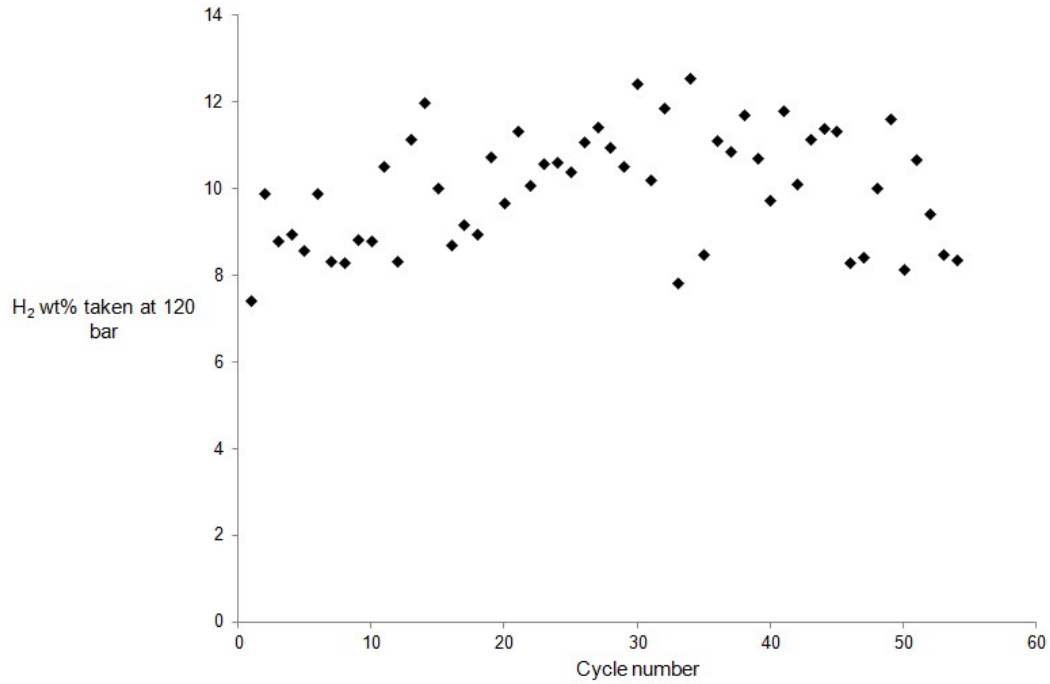

Fig. S16. Cycle of 54 excess hydrogen adsorption and desorption isotherms up to 120 bar recorded at 298 K for KMH-1 after 1st hydrogenation after scaling all values to the

final weight to account for the decrease in mass from 43 mg to 22 mg. This is a different scaling method than that used in Fig. 3B, which assumes gradual weight loss over the 54 cycles. Random scatter is due to shorter equilibration times (1 min) and greater ΔP (30) used during cycling. Average excess adsorption at 120 bar was 10.5 wt%, corresponding to 2.4 mmol H_2, enough to establish high confidence in the storage results, despite the relatively low sample mass.

Density Measurements:

A fluid (xylene) displacement method was used in an argon glove box to measure the density of the materials using ca. 500 mg of material per 20 mL of solvent in a specially designed glass tube with a bulb at the bottom and narrow neck for improved accuracy and calibrated against a standard sand sample of similar weight and known density. Because hydrogenation did not make an appreciable difference in the measured density between **KMH-1 after 1st hydrogenation** (1.86 g cm^{-3}) and **KMH-1 after 2nd hydrogenation** (1.88 g cm^{-3}), the density of **KMH-1 after 2nd hydrogenation** was used as a reasonable density estimate in the volumetric storage calculations for **KMH-1 after cycling**, which at this stage of our research is only available in quantities under 100 mg. Taking into account the differences in packing between crystalline and amorphous structures, and the expected limited penetration of xylene into micropores, the measured density of 1.88 g cm^{-3} is reasonable considering the molecular weight of MnH_2 (56.95 g mol^{-1}) and the density of its third row congener CaH_2 of 1.70 g cm^{-3}, which possesses a molecular weight of only 42.09 g mol^{-1}. Assuming a similar close-packed structure, on the basis of differences in molecular weight alone, we would expect MnH_2 to have a density of 2.3 g mol^{-1}.

Calorimetry:

Calorimetry data was collected using a reaction, scanning and isotherm C80 calorimeter manufactured by Setaram. Two high-pressure cells were used, one for the sample and one as a reference and the cells were linked to the PCT-Pro via a stainless steel gas line with connections manufactured by Swagelok. This allows the recording of an isotherm simultaneously with the *in-situ* calorimetry measurement. The instrument set-up was calibrated by measuring the enthalpy of hydrogen adsorption of 540 mg of palladium. A PCT hydrogen adsorption measurement of palladium up to 6 bar was taken simultaneously to an isothermal calorimetry measurement at 443 K. The total heat of adsorption of palladium as measured and calculated was 31.6 kJ mol^{-1} H_2, which is in line with literature values (*46*). For a measurement, powder was placed in the sample cell with stainless steel spacers to reduce the void space. Identical spacers were also placed in the reference cell. Prior to the measurement the void space of the cells and gas line were determined using a helium volume calibration – one at room temperature and one with the cells in the C80 furnace at 313 K. A hydrogen adsorption measurement was set up using the PCT Pro apparatus with a dose time for each addition of hydrogen gas to the sample set to 60 minutes. This is to allow for thermal equilibration before the hydrogen adsorption measurement moves onto the next dose. The C80 calorimeter was set to take an isothermal measurement of the heat flow of the sample during the PCT measurement with the temperature of the furnace kept constant at 313 K. A calorimetry measurement of a blank cell was also conducted at 313 K simultaneously as a hydrogen adsorption measurement of the blank cell. This was to determine the heat flow during warming of the gas when it is introduced into the cells at different pressures. The total heat of the blank run was

subtracted from the total heat of the sample in every case. To determine the average hydrogen adsorption enthalpy across the range of pressure used in the experiment this value was then divided by the total number of moles of hydrogen adsorbed by the material. For consistency with the excess adsorption measurements, a 200 mg carbon AX-21 sample was used to establish the accuracy and overall veracity of the measurements at the 2 mmol total adsorption level and further details are discussed in the results and discussion section of the manuscript.

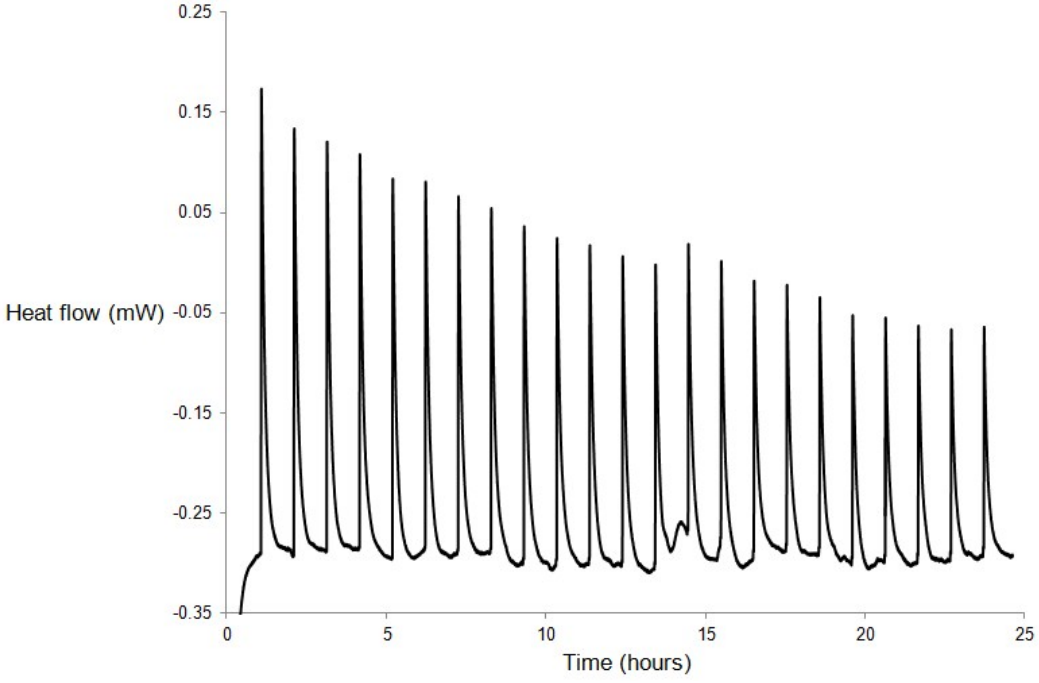

Fig. S17. Calorimetric curves of carbon AX-21 during each dose of H_2 during a PCT hydrogen adsorption measurement recorded at 313 K with 2 mmol of total excess hydrogen adsorption. The pressure was increased linearly from 0-120 bar over the 25 h measurement period.

Inelastic Neutron Scattering (INS):

Inelastic neutron scattering spectra for H_2 were collected on the cold neutron time-of-flight spectrometer FOCUS of the Swiss neutron source SINQ at the Paul Scherrer Institut, Villigen, Switzerland, using 400 mg of the as-received sample with an incident neutron wavelength of 2 Å. The sample as originally received was evacuated and transferred under He atmosphere to the sample can, which was then mounted in the cryostat for data collection. This sample did not, however, take up appreciable amounts of hydrogen when exposed *in-situ* to 67 bar hydrogen pressure at room temperature from an external gas handling system. It was therefore re-activated at 150 °C under dynamic vacuum, which created a relatively small number of active sites. While INS measurements are not quantitative, we must caution that KMH-1 samples left in the glove box for periods of several hours or transported must be reactivated by thermal treatment under vacuum due to adsorption of ambient gas molecules. Unless exposed to water or oxygen such reactivated samples typically retain their original performance. This behavior is typical of hydrogen storage materials possessing high surface areas such as carbon AX-21 (*25*). Furthermore, many organometallic Mn (I) complexes bind dinitrogen more strongly than H_2 (*30*), such that even exposure to trace amounts of nitrogen may lower the number of sites on KMH-1 available for dihydrogen coordination.

Additional Computational results:

Gradual Loading on Mn(II)H_2

Successive H_2 units also bind in a side-on manner to the MnH_2 structure, up to a maximum of five. The HBE gradually decreases with increasing H_2 loading down to

9.0 kJ mol^{-1} per H_2 unit. The enthalpy fluctuates slightly as H_2 loading increases, maximizing at 5.3 kJ mol^{-1} per H_2 with two H_2 present, and finally reaching 4.8 kJ mol^{-1} per H_2, very similar to that seen for a single H_2.

Single loading on M_5H_{10}

In order to better mimic the H_2 binding sites within the KMH-1 family, the computational model was initially extended to a pentameric all-Mn(II) Mn_5H_{10} base structure. Optimisation of several starting structures yielded a most stable geometry for this base structure with a mixture of bridging and terminal hydrides. Multiple sites on the pentameric base structure are available for H_2 binding, and yield HBEs in the range 6.7 to 15.0 kJ mol^{-1}; the corresponding enthalpies range from 2.7 to 10.6 kJ mol^{-1} per H_2, all of them being approximately 4 kJ mol^{-1} lower than the corresponding HBEs, and most likely too low to account for the observed hydrogen uptake at 298 K for KMH-1.

Loading on Mn(I)H

A single H_2 binding to Mn(I)H gave an HBE of 53.8 kJ mol^{-1} (52.8 kJ mol^{-1} at the enthalpic level), very consistent with 52.2 kJ mol^{-1} calculated from hydrogen storage experiments of an organometallic Mn (I) complex (*45*). This binding energy is much higher than that seen experimentally and, as the energies computed from the completely Mn(II) systems are lower than suggested by experiment, we therefore proceeded to examine KMH-1 models incorporating varying numbers of formal Mn(I) centers in pentameric models.

Mn_5H_{10-n} base structures

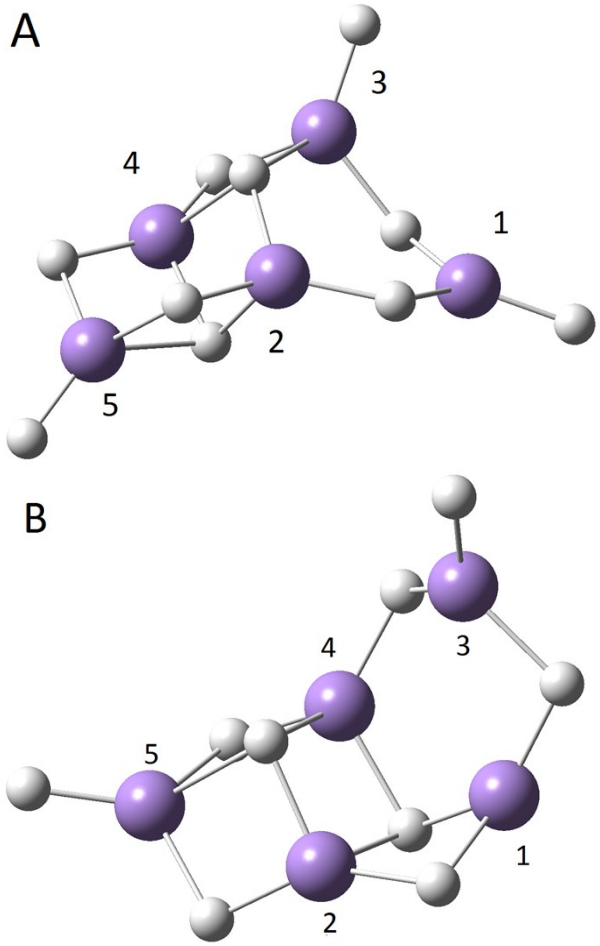

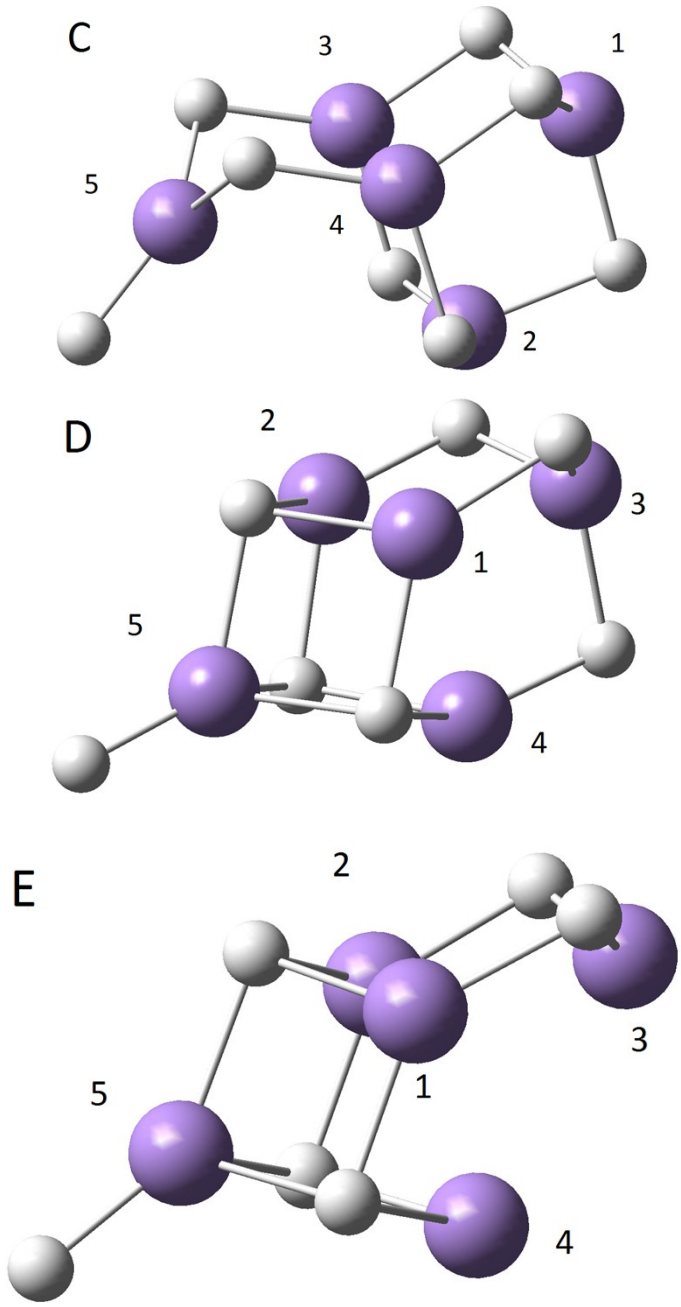

Fig. S18. Optimized geometries of Mn_5H_{10-n}; n=0-4, A to E base structures.

Purple: Mn, Gray: H

Mn_5H_5

An all-Mn(I) pentameric Mn_5H_5 base structure was generated by allowing a ring of alternating Mn and H atoms to relax into a minimum energy state. Note that this

structure contains no terminal hydrides. H_2 was found to dissociate when introduced to this pure Mn(I) model. This is not seen experimentally and, together with the lack of terminal hydrides, leads us to conclude that a Mn_5H_5 model system is not representative of KMH-1.

Natural Charges and Natural Population Analysis

To try to identify the formally Mn(I) and Mn(II) centers in our reduced models we conducted Natural Population Analysis using the NBO6 code (*47*), and the data are given in Table S4. In all cases, the absolute values of the NBO charges are significantly different from the formal oxidation states (not atypical behavior), but we hoped that the relative values would provide insight into charge localization. In the first two Mn(I)-containing structures there appears to be little such localization, but as the amount of formal Mn(I) increases it could be argued that center 5 looks increasingly different from the rest, being more Mn(I)-like; this observation is consistent with the geometries as there is a terminal hydride on this center.

Table S4. Natural charge and valence populations for the pentameric base structures, with the Mn centers (1–5) labeled in Figure S18A-E

Base Structure		**1**	**2**	**3**	**4**	**5**	**Max-min**
Mn_5H_{10}–S18A	Natural Valence Population	0.56	0.59	0.63	0.58	0.62	0.07
	Natural Charge	2.94	2.89	2.87	2.90	2.87	0.07
Mn_5H_9-S18B	Natural Valence Population	0.77	0.78	0.67	0.83	0.62	0.21

	Natural Charge	2.70	2.70	2.81	2.63	2.87	0.24
Mn_5H_8-S18C	Natural Valence Population	0.78	0.91	0.95	0.91	0.73	0.22
	Natural Charge	2.69	2.55	2.51	2.55	2.76	0.25
Mn_5H_7-S18D	Natural Valence Population	1.19	1.03	1.00	1.03	0.77	0.42
	Natural Charge	2.26	2.44	2.47	2.44	2.71	0.45
Mn_5H_6-S18E	Natural Valence Population	1.32	1.33	1.14	1.11	0.83	0.50
	Natural Charge	2.14	2.13	2.33	2.35	2.65	0.52

Orientation of H_2 on pentamers

The Kubas-like orbital mechanism requires that H_2 binds side on to the Mn centers to facilitate back donation into the dihydrogen σ* orbital. As described above in the computational methodology section, to establish such binding we calculate the difference between the Mn-H (H_2) distances for each H_2 unit. At the extremes of our range of model base structures, Mn_5H_{10} and Mn_5H_6, a loading of two H_2 per Mn gives nine H_2 oriented to undergo an orbital interaction for the former, and five Kubas-bound H_2 for the latter. These five H_2 are in approximately the same positions as those for Mn_5H_6 with one H_2 per Mn, implying that the first five H_2 bind to this base structure in a Kubas manner, with subsequent H_2 being physisorbed. The reduction in the number of Kubas-like H_2 from Mn_5H_{10} to Mn_5H_6 is most likely due to a reduction in the volume available around each Mn center on the smaller base structure; in the latter, the first few H_2 bind more strongly and lie closer to the Mn (1.7 – 2.1 Å vs 2.7-3.4 Å in Mn_5H_{10}). This conclusion is consistent with the H_2 binding energy data presented below.

Breakdown of H-H distance data

To gain greater insight into the behaviour of the Kubas and physisorbed H_2 units, we have analysed the H-H distances for the H_2 molecules within each group. The average H-H distances for the two groups are presented in Fig. 5. For the non-Kubas binding H_2, these distances are essentially unaltered as the amount of Mn(I) increases, especially for the series with a total of 10 H_2 bound (between 0.755 and 0.757 Å); this is consistent with physisorption having little effect on the H-H bond length. Although the Mn_5H_{10} structure shows little difference between the Kubas and non-Kubas bound H_2, the systems with greater amounts of Mn(I) present show larger Kubas bound H-H bond distance increases. Hence the overall trend towards longer average H-H distances with increasing amounts of Mn(I) can be traced to the stronger Kubas binding in these systems.

Example INS energy against rotation plot

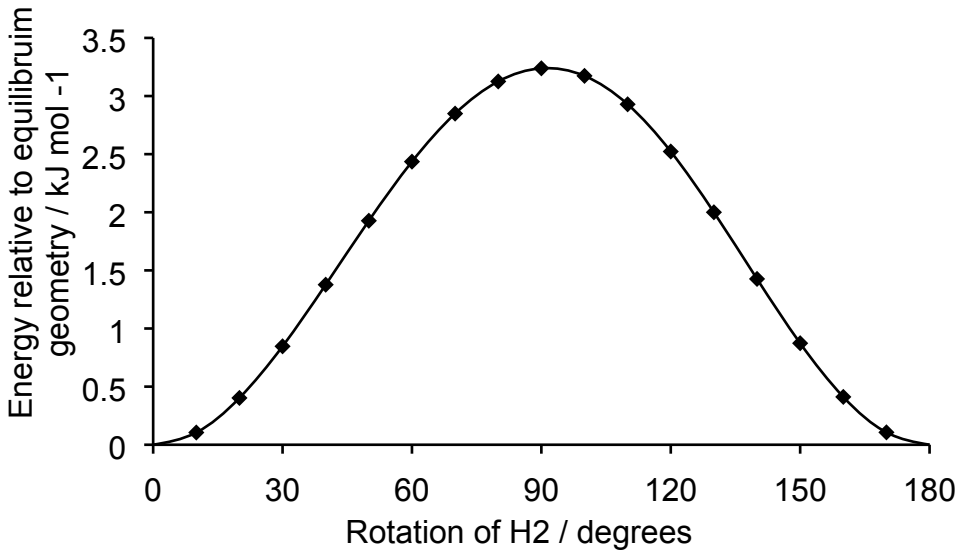

Fig. S19. Energy profile for the rotation of a single H_2 molecule on the Mn_5H_{10} base structure with five H_2 molecules bound.

Loaded Mn5H6 with anomalies highlighted

When H_2 is added to the Mn_5H_6 BSM we find that two of the H_2 display much stronger binding motifs than the other H_2 even though they are both predominantly bound to the same Mn, highlighted in Fig. S20. The highlighted H_2 on the left has its bond length extended to 0.828 Å which is 0.032 Å greater than the longest of the non-highlighted H_2. The highlighted H_2 on the right is extended even more, to 0.973 Å, and is strongly held in its orientation, this is presented as an anomaly in Table 4. The reason that the H_2 highlighted on the right is much more extended and held in its current orientation is that the H atom in yellow forms a bridge between two of the Mn atoms and so it is energetically favorable for the H atom to be displaced into the region as much as possible and kept there: the gap where the bridge is produced is occupied by a base structure H atom in Mn_5H_7.

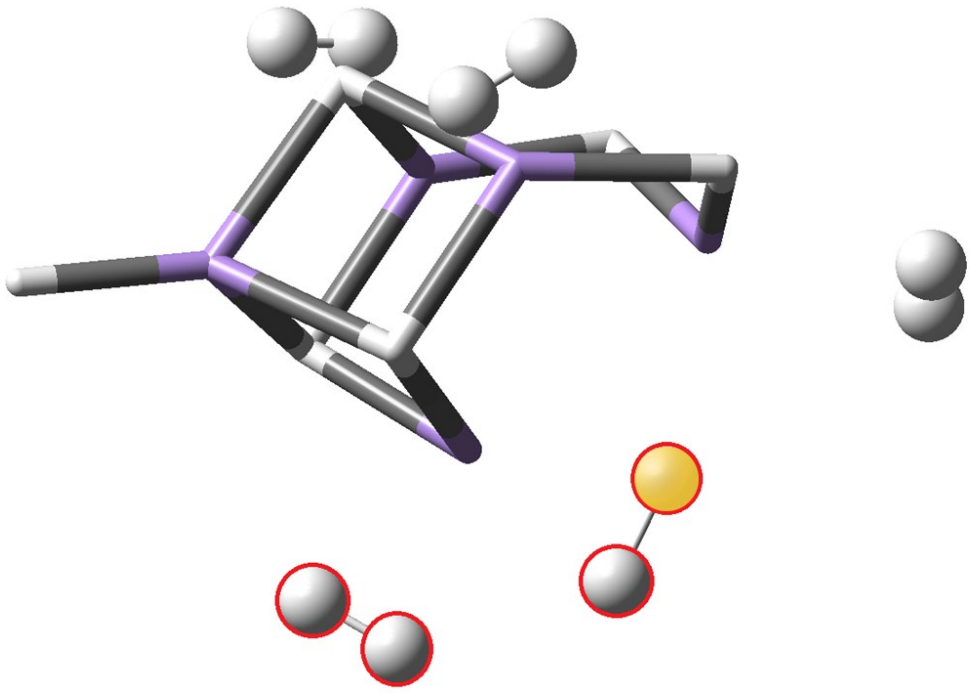

Fig. S20. Optimised structure of Mn_5H_6 with a loading of 1 H_2 per Mn. Purple: Mn, Gray: H. External H_2 represented as balls. Red highlighted H_2 have a much greater extension than the others. Yellow hydrogen bridges two of the Mn.

Table S5. Cartesian Coordinates of MnH_2**.n**H_2 Optimized Geometry: SCF Energy, *Hydrogen Binding Energy (kJ mol^{-1}),* **Hydrogen Binding Enthalpy (kJ mol^{-1})**

n=0, -1151.8702058

Mn	0.000000	0.000000	0.015197
H	0.000000	1.668534	-0.189960
H	0.000000	-1.668534	-0.189960

n=1, -1153.0400250, *10.4*, **4.6**

Mn	0.000000	0.000000	0.185326
H	0.000000	1.653894	-0.085447
H	0.000000	-1.653894	-0.085447
H	0.000000	-0.382175	-2.231129
H	0.000000	0.382175	-2.231129

n=5, -1157.7166805, *9.0*, **4.8**

Mn	0.000000	0.017653	0.000000
H	-0.000093	-0.218616	1.667936
H	-0.000093	-0.218616	-1.667936
H	-1.558484	-2.168896	0.379166
H	-1.558484	-2.168896	-0.379166
H	1.552848	-2.172880	-0.379166
H	1.552848	-2.172880	0.379166
H	2.574740	0.811378	0.378853

H 2.574740 0.811378 -0.378853

H -2.572615 0.818184 -0.378853

H -2.572615 0.818184 0.378853

H 0.003604 2.710167 -0.378802

H 0.003604 2.710167 0.378802

Table S6. Cartesian Coordinates of MnH**.n**H_2 Optimized Geometry: SCF Energy, *Hydrogen Binding Energy (kJ mol^{-1}),* **Hydrogen Binding Enthalpy (kJ mol^{-1})**

n=0, -1151.2619093

Mn 0.000000 0.000000 0.061169

H 0.000000 0.000000 -1.529233

n=1, -1152.4482426, *53.8*, **52.8**

Mn 0.000000 0.057225 0.000000

H -0.000010 1.701634 0.000000

H -0.473284 -1.566136 0.000000

H 0.473293 -1.566133 0.000000

Table S7. Cartesian Coordinates of Mn_5H_{10}**.n**H_2 Optimized Geometry: SCF Energy, *Hydrogen Binding Energy (kJ mol^{-1}),* **Hydrogen Binding Enthalpy (kJ mol^{-1})**

n=0, -5759.6125851

Mn	2.578675	-1.439752	-0.443941
H	1.133270	-2.138839	0.454560
Mn	-0.283548	-1.120931	0.674036
H	3.840137	-2.372418	-0.939424
H	2.282542	0.312786	-0.709174
H	-1.949983	-1.488977	1.148548
Mn	1.724944	1.724105	0.304738
H	0.338664	2.533980	-0.665977
Mn	-1.015938	1.443804	-0.415610
H	0.099019	0.694882	1.002377
H	2.704148	2.546099	1.341801
H	-1.074710	-0.403052	-0.930125
H	-2.733402	1.267617	-0.023832
Mn	-3.014766	-0.595531	-0.115410
H	-4.373872	-1.244445	-0.774070

n=1, -5760.7817522, *8.7*, **4.7**

Mn	2.661688	-1.435880	-0.358880
H	1.195886	-2.141052	0.495949
Mn	-0.254329	-1.162075	0.663879
H	3.935605	-2.386201	-0.786171
H	2.463052	0.320881	-0.656664
H	-1.906353	-1.530400	1.183483
Mn	1.695502	1.729193	0.198938
H	0.325892	2.384840	-0.900738

Mn	-1.043526	1.352412	-0.513432
H	0.107874	0.668673	0.904771
H	2.458352	2.732025	1.261981
H	-1.076499	-0.531378	-0.953218
H	-2.759025	1.156255	-0.115640
Mn	-2.997265	-0.715044	-0.114436
H	-4.356662	-1.416020	-0.716675
H	-0.593568	3.293213	1.664036
H	-1.346311	3.233994	1.717159

n=1, -5760.7841389, *15.0*, **10.6**

Mn	2.608147	-1.319783	-0.491721
H	1.165187	-2.116269	0.328671
Mn	-0.278448	-1.143372	0.564206
H	3.894968	-2.184505	-1.044344
H	2.091528	0.369760	-0.873833
H	-1.912400	-1.577494	1.102733
Mn	1.610419	1.737895	0.234245
H	0.170654	2.590841	-0.603241
Mn	-1.148270	1.449394	-0.353998
H	0.048005	0.669458	0.978129
H	2.669983	2.395279	1.316490
H	-1.173633	-0.368740	-0.960429
H	-2.837915	1.200133	0.106565
Mn	-3.061724	-0.667072	-0.068026

H -4.428220 -1.325830 -0.701853

H 3.670306 -0.894243 1.641757

H 3.388422 -0.184907 1.591708

n=1, -5760.7809910, *6.7*, **2.7**

Mn 2.446223 -1.631849 -0.419253

H 0.925963 -2.277139 0.389499

Mn -0.429774 -1.180826 0.621634

H 3.680620 -2.614663 -0.886637

H 2.239070 0.136755 -0.654081

H -2.127052 -1.469260 1.043108

Mn 1.790502 1.554599 0.403136

H 0.451656 2.500659 -0.506532

Mn -0.968059 1.484394 -0.315089

H 0.075880 0.580405 1.053805

H 2.807652 2.236418 1.507846

H -1.142206 -0.318861 -0.949070

H -2.701578 1.401504 0.034154

Mn -3.103016 -0.429733 -0.180078

H -4.489730 -0.940329 -0.900697

H 3.573360 3.023498 -1.104778

H 3.309454 2.826396 -1.785347

n=1, -5760.7832050, *12.5*, **10.0**

Mn -0.834148 1.872923 -0.922243

H	-0.306744	2.173189	0.864674
Mn	0.467917	0.690034	1.375490
H	-0.716659	3.010803	-2.105995
H	-2.201660	0.691692	-0.762555
H	2.196740	0.339093	1.409798
Mn	-2.486416	-0.846896	0.152084
H	-1.477632	-2.065609	-0.882574
Mn	0.153017	-1.524387	-0.551394
H	-0.588792	-0.836716	1.110824
H	-3.823271	-1.250417	1.023210
H	0.716137	0.376842	-0.710764
H	1.876011	-1.914472	-0.566355
Mn	2.721684	-0.261159	-0.287033
H	4.153938	0.146683	-0.976356
H	-0.436693	0.260429	3.614214
H	0.057289	0.805611	3.809278

n=1, -5760.7812306, *7.3*, **3.3**

Mn	2.661959	-1.440544	-0.384551
H	1.182413	-2.142793	0.452117
Mn	-0.242322	-1.126168	0.619500
H	3.923274	-2.385522	-0.858184
H	2.425912	0.323880	-0.616400
H	-1.920731	-1.494137	1.043365
Mn	1.781291	1.723935	0.359487

H	0.448926	2.520553	-0.696192
Mn	-0.916027	1.431457	-0.512937
H	0.125922	0.690276	0.967580
H	2.685697	2.567914	1.446444
H	-0.955696	-0.410420	-1.009909
H	-2.647452	1.282683	-0.178870
Mn	-2.959819	-0.575860	-0.223368
H	-4.300706	-1.221044	-0.928413
H	-4.296018	0.137757	2.193145
H	-4.798581	-0.189649	1.732035

n=5, -5765.4591467, *9.1*, **5.1**

Mn	2.625608	-1.485839	-0.447345
H	1.066531	-2.260631	0.134577
Mn	-0.351178	-1.245672	0.358784
H	3.926054	-2.407548	-0.864396
H	2.355659	0.259983	-0.794609
H	-2.018421	-1.623654	0.828281
Mn	1.714320	1.585998	0.269335
H	0.369712	2.481337	-0.670332
Mn	-1.033878	1.436447	-0.462916
H	0.073584	0.524243	0.843020
H	2.540162	2.206491	1.564717
H	-1.148329	-0.348151	-1.158597
H	-2.747457	1.278414	-0.048270

Mn	-3.085277	-0.562981	-0.293805
H	-4.481962	-1.100049	-0.982570
H	-4.301428	-0.085208	2.286592
H	-4.833916	-0.340922	1.814546
H	-0.493663	2.948404	2.073863
H	-1.249509	2.956010	2.101455
H	0.456266	-0.819681	3.069218
H	0.362918	-1.560061	3.189408
H	3.422707	-1.221991	1.848527
H	3.179565	-0.499427	1.796451
H	3.490837	3.299281	-0.963983
H	3.290818	3.114317	-1.669235

n=10, -5771.3039456, *8.6*, **3.9**

Mn	-2.583575	-1.492454	0.492697
H	-1.198566	-2.204586	-0.479231
Mn	0.184470	-1.157691	-0.775454
H	-3.782907	-2.451640	1.093228
H	-2.358584	0.269756	0.756516
H	1.847636	-1.491131	-1.296654
Mn	-1.798983	1.639694	-0.293895
H	-0.419878	2.467535	0.656410
Mn	0.966806	1.417976	0.332067
H	-0.202872	0.662157	-1.065847
H	-2.758305	2.389533	-1.414922

H	1.012181	-0.445449	0.830903
H	2.684863	1.211112	-0.089138
Mn	2.907708	-0.656384	0.004642
H	4.187950	-1.396091	0.739700
H	4.363461	-0.030392	-2.425319
H	4.836953	-0.378709	-1.949878
H	0.592989	3.262981	-1.913890
H	1.345262	3.210467	-1.968378
H	-0.884962	-0.551725	-3.326292
H	-0.822684	-1.282657	-3.509544
H	-3.735682	-1.088756	-1.838574
H	-3.530715	-0.361832	-1.745142
H	-3.538197	3.249033	1.194681
H	-3.335715	3.049768	1.894880
H	-1.188959	-1.906396	2.722508
H	-0.630309	-1.529789	2.371331
H	1.737933	-3.296878	1.047321
H	1.033849	-3.570466	1.028978
H	1.427198	1.879445	3.057575
H	1.800899	1.224587	2.994753
H	2.867604	-1.403652	2.972218
H	2.393506	-1.393207	3.560548
H	2.523080	3.926209	1.025934
H	1.822334	4.202239	1.073911

Table S8. Cartesian Coordinates of Mn_5H_9**.n**H_2 Optimized Geometry: SCF Energy, *Hydrogen Binding Energy (kJ mol^{-1}),* **Hydrogen Binding Enthalpy (kJ mol^{-1})**

n=0, -5759.0575902

Mn	1.584328	-1.390838	-0.429851
H	0.540901	-2.475979	0.580683
Mn	-0.905944	-1.417690	0.443921
H	3.018180	-0.516992	-0.020380
H	-2.644171	-1.281605	0.227961
Mn	2.407702	1.158762	0.552890
H	1.278676	1.968441	-0.651440
Mn	-0.160627	0.975499	-0.784524
H	-0.847318	0.375858	0.858813
H	3.117018	1.842019	1.873641
H	-0.028449	-0.882653	-1.254643
H	-1.830154	1.411617	-1.171062
Mn	-2.864084	0.603120	0.163704
H	-4.139049	1.337968	0.902911

n=5, -5764.907627, *10.9*, **6.6**

Mn	-1.447965	1.437733	-0.484510
H	-0.347766	2.477398	0.513378
Mn	1.050379	1.355192	0.427548
H	-2.938146	0.708926	0.006057
H	2.770535	1.144955	0.107907

Mn	-2.596469	-1.033269	0.509183
H	-1.311164	-2.043484	-0.290120
Mn	0.120486	-1.072270	-0.589299
H	0.990083	-0.420895	0.958910
H	-3.731997	-1.719984	1.500112
H	0.125926	0.733510	-1.225313
H	1.742586	-1.586437	-1.088002
Mn	2.911442	-0.749800	0.115449
H	4.224566	-1.502573	0.777148
H	1.134341	1.851856	3.189152
H	1.345424	1.127370	3.130215
H	-1.846781	-0.389486	2.709412
H	-1.255057	-0.098566	2.318079
H	-1.755066	2.762496	-2.093201
H	-1.037486	2.511126	-2.245269
H	-4.264344	-1.744812	-1.471441
H	-3.727667	-1.586166	-1.981223
H	4.221718	-0.154720	-2.363364
H	4.713451	-0.510175	-1.911724

n=10, -5770.751893, *9.4*, **4.4**

Mn	-1.601092	1.519568	0.023338
H	-0.539252	2.181738	1.339958
Mn	0.897286	1.204676	0.888698
H	-3.010333	0.547257	0.237292

H	2.623434	1.223461	0.515809
Mn	-2.453629	-1.225455	0.242764
H	-1.286568	-1.761037	-1.063775
Mn	0.100504	-0.691161	-1.002640
H	0.933522	-0.630980	0.686074
H	-3.322467	-2.270751	1.191491
H	-0.000242	1.208331	-0.899243
H	1.740477	-0.860865	-1.650237
Mn	2.854510	-0.522268	-0.187278
H	4.158377	-1.471653	0.190115
H	2.515479	-2.167702	2.986615
H	2.974576	-2.009648	2.406891
H	1.052842	0.795174	3.605263
H	1.440965	0.196180	3.352621
H	1.540859	-3.656023	-0.079411
H	2.239576	-3.368894	-0.047316
H	-1.952312	-0.596429	2.933198
H	-1.466951	-0.080651	2.660077
H	-1.979287	3.291652	-1.055483
H	-1.252299	3.135140	-1.274953
H	-4.415414	-1.684888	-1.426805
H	-4.084339	-1.280159	-1.975134
H	-2.124552	0.498107	-2.753685
H	-2.419866	0.836558	-3.362493
H	1.728372	2.232239	-2.345281

H	2.027044	2.712931	-2.844280
H	4.188714	1.006438	-2.183491
H	4.683202	0.509242	-1.899282
H	-0.804181	-2.994951	1.873488
H	-0.128865	-2.673823	1.759934

Table S9. Cartesian Coordinates of Mn_5H_8**.n**H_2 Optimized Geometry: SCF Energy, *Hydrogen Binding Energy (kJ mol^{-1}),* **Hydrogen Binding Enthalpy (kJ mol^{-1})**

n=0, -5758.500288

Mn	2.203366	0.000003	0.592363
H	1.475298	1.490223	1.301183
Mn	-0.138448	1.526404	0.475460
H	2.437413	0.000000	-1.182921
H	-1.813742	1.461357	0.987495
Mn	0.617432	-0.000005	-1.615394
H	0.169952	-1.666928	-1.318837
Mn	-0.138448	-1.526403	0.475467
H	0.169950	1.666919	-1.318842
H	1.475300	-1.490217	1.301187
H	-1.813742	-1.461351	0.987502
Mn	-2.481794	0.000001	0.085080
H	-3.653126	-0.000001	-1.081166

n=5, -5764.354942, *13.3*, **8.7**

Mn	1.926272	-0.000006	-1.088378
H	1.056641	-1.498212	-1.508747
Mn	-0.252826	-1.517309	-0.231950
H	2.711175	0.000002	0.546318
H	-1.980214	-1.587988	-0.585322
Mn	1.159308	0.000004	1.533162
H	0.385536	1.590946	1.471547
Mn	-0.252825	1.517308	-0.231960
H	0.385534	-1.590935	1.471560
H	1.056642	1.498198	-1.508758
H	-1.980212	1.587981	-0.585343
Mn	-2.728683	0.000000	-0.185685
H	-4.346696	0.000003	0.215254
H	-1.957624	0.000003	1.917354
H	-2.727293	0.000004	2.018847
H	2.044807	0.000046	3.436084
H	2.659090	0.000043	2.963040
H	0.052373	-3.920177	-0.115236
H	-0.672855	-3.857079	-0.339354
H	0.052358	3.920179	-0.115251
H	-0.672865	3.857073	-0.339385
H	3.970286	0.000006	-1.551931
H	3.682171	-0.000001	-2.270416

n=10, -5770.198785, *10.5*, **5.2**

Mn	1.749787	0.347283	1.188876
H	0.791612	1.842427	1.068384
Mn	-0.325576	1.440120	-0.318836
H	2.762439	-0.036354	-0.267666
H	-2.083909	1.483023	-0.250374
Mn	1.370799	-0.398798	-1.405806
H	0.620894	-1.955909	-1.026006
Mn	-0.230869	-1.486614	0.512342
H	0.530629	1.081526	-1.888398
H	0.881640	-1.039509	1.889718
H	-1.985575	-1.583687	0.641406
Mn	-2.727118	-0.195499	-0.232552
H	-4.254505	-0.429535	-0.864418
H	-3.858575	0.555871	2.297569
H	-4.365021	0.376391	1.763786
H	-1.619401	-0.736929	-2.241262
H	-2.361682	-0.815051	-2.434670
H	3.106983	3.213603	-1.088387
H	2.766553	2.555755	-0.939194
H	2.530623	-0.844641	-3.088222
H	3.064907	-0.680069	-2.549914
H	0.063812	3.577864	-1.328319
H	-0.516217	3.776575	-0.876538
H	0.264974	-3.804409	1.005170

H	-0.467656	-3.764398	1.209019
H	-0.962391	3.482948	1.882012
H	-1.460868	4.045546	1.949540
H	-1.069173	0.647607	2.716164
H	-1.492430	0.882254	3.297008
H	3.706388	0.601640	1.822832
H	3.340381	0.776185	2.484372
H	3.260386	-3.243951	0.714528
H	2.879592	-2.627099	0.501276

Table S10. Cartesian Coordinates of Mn_5H_7**.n**H_2 Optimized Geometry: SCF Energy, *Hydrogen Binding Energy (kJ mol^{-1}),* **Hydrogen Binding Enthalpy (kJ mol^{-1})**

n=0, -5757.914581

Mn	0.119376	-0.000003	1.485299
Mn	0.017237	1.385354	-0.737361
H	1.880141	-0.000004	1.748031
H	-1.068055	1.314430	0.790788
Mn	2.174050	0.000000	-0.021460
H	1.745321	-1.407879	-1.135887
Mn	0.017236	-1.385352	-0.737366
H	-1.115426	0.000003	-1.515736
H	1.745321	1.407879	-1.135886
H	-1.068054	-1.314433	0.790785

Mn	-2.256684	0.000001	0.021747
H	-3.899617	-0.000011	0.186442

n=5, -5763.778442, *18.2*, **13.2**

Mn	0.023186	-0.947999	-1.206702
Mn	0.052268	-0.536301	1.400983
H	1.761411	-0.789953	-1.504066
H	-1.059524	-1.523837	0.223335
Mn	2.133549	0.157192	0.016169
H	1.624705	1.890069	-0.339146
Mn	-0.123323	1.610771	-0.171143
H	-1.173626	0.924921	1.222324
H	1.806710	-0.495963	1.650565
H	-1.156994	0.564868	-1.414494
Mn	-2.320754	-0.065744	-0.002875
H	-3.972373	-0.186591	0.033932
H	-0.077643	-1.329902	3.290781
H	-0.833755	-1.293361	3.115098
H	-0.214510	3.572619	-0.605663
H	-0.969416	3.386514	-0.698334
H	1.549197	-3.824587	0.153187
H	1.472618	-3.070728	0.191426
H	-0.060450	-2.247197	-2.755128
H	-0.817366	-2.064591	-2.691859
H	4.063468	0.141406	-0.471805

H 3.934411 0.898335 -0.310957

n=10, -5769.621851, *12.8*, **6.9**

Mn 0.128991 1.369547 -0.634398

Mn 0.031980 -0.240691 1.479037

H -1.607802 1.763891 -0.658461

H 1.322346 0.953495 0.744305

Mn -2.171344 0.257331 0.216366

H -2.086561 -1.093705 -1.016466

Mn -0.336244 -1.354000 -0.899110

H 0.886326 -1.642312 0.513875

H -1.682096 -0.049400 1.906672

H 0.909073 -0.116513 -1.661509

Mn 2.190124 -0.462577 -0.281945

H 3.848645 -0.460031 -0.277641

H -1.742741 -2.914266 1.086607

H -1.859019 -3.654850 1.200213

H 0.357842 -0.377988 3.518078

H 1.091158 -0.427066 3.271129

H -1.495888 0.741946 -3.867398

H -1.609359 0.611986 -3.131562

H -0.641674 -2.993274 -2.028168

H 0.128454 -2.897939 -2.131142

H 0.754114 4.111459 0.381113

H 1.188826 3.568337 0.677432

H	0.136325	2.874043	-2.024698
H	0.816288	2.530971	-2.188363
H	-3.992287	0.982039	-0.056557
H	-4.117144	0.213057	-0.151470
H	-0.473587	2.808732	3.095731
H	-0.709907	2.334171	2.554921
H	3.711723	-0.559042	2.354172
H	3.725108	-0.607047	3.109153
H	3.505154	2.893834	-1.208496
H	3.549022	2.165200	-1.010228

Table S11. Cartesian Coordinates of Mn_5H_6**.n**H_2 Optimized Geometry: SCF Energy, *Hydrogen Binding Energy (kJ mol^{-1}),* **Hydrogen Binding Enthalpy (kJ mol^{-1})**

n=0, -5757.314743

Mn	0.144597	-1.333819	0.628865
Mn	0.132772	1.335412	0.612902
H	1.898722	-1.604586	0.721122
H	-0.817304	0.004632	1.544754
Mn	2.163101	0.005741	0.019928
Mn	-0.102170	-0.012072	-1.553523
H	-1.175768	1.355676	-0.661360
H	1.881256	1.623816	0.695853
H	-1.158515	-1.356545	-0.643187
Mn	-2.210810	0.010716	0.229871

H -3.815654 -0.172458 -0.108261

n=5, -5763.185849, *22.0*, **17.1**

Mn 0.043787 -1.082206 -1.128258

Mn 0.069291 -0.434154 1.460113

H 1.789217 -1.029192 -1.417343

H -1.023060 -1.548452 0.362847

Mn 2.144955 -0.042091 0.065960

Mn -0.078039 1.565603 -0.298676

H -1.070756 0.968434 1.123139

H 1.827057 -0.501033 1.739010

H -1.127307 0.366471 -1.452304

Mn -2.290881 -0.101301 0.003800

H -3.931207 0.003509 0.184142

H 0.127428 -1.092372 3.350587

H -0.635102 -1.180185 3.202302

H -0.258150 -2.434773 -2.628777

H -0.940936 -2.055759 -2.622465

H 1.503268 1.776659 -0.880006

H 0.996504 2.571606 -1.121042

H -0.824591 3.145522 -0.743311

H -1.422592 2.795842 -0.290635

H 3.970478 0.537294 -0.401041

H 3.791915 0.030141 -0.978553

n=10, -5769.029614, *14.8*, **8.7**

Mn	-0.314722	-1.463849	-0.442350
Mn	0.144481	0.327343	1.505298
H	1.364913	-1.958677	-0.704081
H	-1.253849	-0.922523	1.110208
Mn	2.044856	-0.448897	0.036547
Mn	0.110091	1.211940	-1.022103
H	-0.803051	1.593187	0.552081
H	1.888628	0.049249	1.724974
H	-1.265449	-0.112508	-1.390261
Mn	-2.290323	0.415358	0.140874
H	-3.898795	0.784967	0.252056
H	0.350663	0.549246	3.492595
H	-0.426731	0.601209	3.434408
H	0.953342	-2.638589	2.110527
H	0.985335	-3.229170	2.584929
H	-1.017249	-3.268655	-1.148559
H	-1.596050	-2.788066	-1.349165
H	0.742789	-1.285851	-3.913595
H	0.896175	-1.331694	-3.174518
H	1.625291	0.743917	-1.648235
H	1.321026	1.490356	-2.175126
H	1.149339	3.353344	0.458211
H	1.316621	4.070331	0.279053
H	-4.245331	-2.534471	-0.592209

H -4.181283 -1.798551 -0.429500

H -0.297010 2.599069 -2.113307

H -0.912194 2.627111 -1.566770

H 3.913615 -0.604995 -0.640505

H 3.577945 -1.276532 -0.872411

H 4.054820 2.246126 -0.007720

H 3.396923 1.994780 0.270252

n=11, -5770.197739, *14.0*, **9.6**

Mn 0.043769 1.489002 -0.560570

Mn -0.190281 -0.175001 1.532062

H -1.683515 1.689338 -0.895330

H 1.008294 1.241879 1.051320

Mn -2.146129 0.163285 -0.030067

Mn 0.053757 -1.259765 -0.901062

H 0.969757 -1.354261 0.713535

H -1.961834 -0.155226 1.698329

H 1.222538 0.229856 -1.366818

Mn 2.264364 0.006661 0.223708

H 3.906366 -0.121924 0.392945

H -0.415960 -0.253194 3.526125

H 0.360989 -0.180170 3.484431

H -1.471114 2.663432 1.845352

H -1.609589 3.282156 2.261258

H 0.471151 3.312259 -1.416966

H	1.127706	2.917766	-1.557980
H	-0.861781	0.874265	-4.018101
H	-1.055249	0.960797	-3.292249
H	-1.488349	-1.085374	-1.607197
H	-1.051029	-1.811203	-2.063116
H	-0.581991	-3.455625	0.763558
H	-0.641758	-4.199544	0.635172
H	3.769419	3.149945	-0.727575
H	3.812589	2.427912	-0.506617
H	0.721673	-2.650628	-1.859020
H	1.306566	-2.538465	-1.293732
H	-3.988158	-0.046447	-0.755162
H	-3.756711	0.648041	-1.041835
H	-3.616059	-2.842822	0.123574
H	-3.017470	-2.455624	0.379577
H	3.938792	-2.568494	-0.414615
H	3.947733	-3.283220	-0.660613